

Annual Review of Biophysics

Super-Resolution Microscopy for Structural Cell Biology

Sheng Liu,* Philipp Hoess,* and Jonas Ries

Cell Biology & Biophysics Unit, European Molecular Biology Laboratory, Heidelberg,
Germany; email: jonas.ries@embl.de

Annu. Rev. Biophys. 2022. 51:301–26

First published as a Review in Advance on
February 4, 2022

The *Annual Review of Biophysics* is online at
biophys.annualreviews.org

<https://doi.org/10.1146/annurev-biophys-102521-112912>

Copyright © 2022 by Annual Reviews.
All rights reserved

*These authors contributed equally to this article

ANNUAL
REVIEWS **CONNECT**

www.annualreviews.org

- Download figures
- Navigate cited references
- Keyword search
- Explore related articles
- Share via email or social media

Keywords

structural biology, cell biology, single-molecule localization microscopy, super-resolution microscopy, MINFLUX, molecular machines

Abstract

Super-resolution microscopy techniques, and specifically single-molecule localization microscopy (SMLM), are approaching nanometer resolution inside cells and thus have great potential to complement structural biology techniques such as electron microscopy for structural cell biology. In this review, we introduce the different flavors of super-resolution microscopy, with a special emphasis on SMLM and MINFLUX (minimal photon flux). We summarize recent technical developments that pushed these localization-based techniques to structural scales and review the experimental conditions that are key to obtaining data of the highest quality. Furthermore, we give an overview of different analysis methods and highlight studies that used SMLM to gain structural insights into biologically relevant molecular machines. Ultimately, we give our perspective on what is needed to push the resolution of these techniques even further and to apply them to investigating dynamic structural rearrangements in living cells.

Contents

INTRODUCTION	302
STRUCTURAL RESOLUTION WITH OPTICAL MICROSCOPY	303
Single-Molecule Localization Microscopy	304
MINFLUX	305
PUSHING SINGLE-MOLECULE LOCALIZATION MICROSCOPY	
TOWARD STRUCTURAL SCALES	306
New Microscopes to Reach Nanometer 3D Resolution	306
Stability	309
Improved Labels for Single-Molecule Localization Microscopy	310
Multicolor Single-Molecule Localization Microscopy	312
Speed and Throughput	313
Dynamic Live-Cell Imaging	313
Counting of Proteins	313
Data Analysis	314
Correlative Single-Molecule Localization Microscopy and Electron Microscopy ...	315
APPLICATION OF SUPER-RESOLUTION MICROSCOPY	
TO STRUCTURAL CELL BIOLOGY	316
CONCLUSION	317

Single-molecule localization microscopy (SMLM):

localization of thousands of sparsely activated fluorophores with nanometer precision over many camera frames; allows reconstruction of a super-resolved image

Stimulated emission depletion (STED) microscopy:

built upon confocal laser scanning microscopy; depletes the fluorescence emission at the periphery of the diffraction-limited area through stimulated emission

INTRODUCTION

The resolution revolution in cryo-electron microscopy (EM) has led to a breakthrough in structural cell biology, allowing us to solve structures of protein complexes in their native environment—the cell. However, to reach the molecular resolution that is necessary to identify individual proteins, many identical structures need to be averaged, which is challenging for dynamic and heterogenous protein assemblies. In addition, the use of vitrified cryo-fixed samples precludes direct measurements of dynamic conformational changes, which instead have to be reconstructed indirectly from a large number of fixed snapshots.

Optical super-resolution microscopy (SRM) methods have the potential to optimally complement classical structural biology techniques, as they can overcome these two major limitations: The use of fluorescent labels leads to molecular specificity and high contrast, allowing meaningful analysis of individual structures without averaging, and in principle, SRM can directly image dynamic structural changes in living cells. The development of SRM, and specifically single-molecule localization microscopy (SMLM) (82) and stimulated emission depletion (STED) microscopy (135), has increased the resolution of fluorescence microscopy by more than one order of magnitude compared to diffraction-limited fluorescence microscopy. The resolution is now comparable to the size of large cellular multiprotein machines but still far from the angstrom resolution of cryo-EM. In fact, SRM can only measure positions of fluorescent labels and thus can never image the entire structure of a protein, and the resolution of SRM will remain limited by the size of the label to approximately one nanometer. However, in combination with information from methods used in structural biology with molecular resolution, SRM has the potential to provide the missing information on conformations of individual complexes and their dynamic changes in the living cell.

In this review, we discuss recent developments that enabled SRM to investigate questions of structural cell biology, i.e., about the structural organization and conformation of proteins and

multiprotein complexes in the cell. We identify the major bottlenecks of current technologies and provide a perspective on how they might be overcome in the near future.

STRUCTURAL RESOLUTION WITH OPTICAL MICROSCOPY

The two main approaches that achieve SRM with nanometer resolution are STED and SMLM. STED is based on confocal laser scanning microscopy (**Figure 1b**): Fluorophores within the diffraction-limited region are excited to a higher-energy state by a Gaussian-shaped excitation beam, followed by a donut-shaped beam that depletes the fluorescence emission at the periphery of the excited fluorophores through stimulated emission. Only the fluorophores close to the center

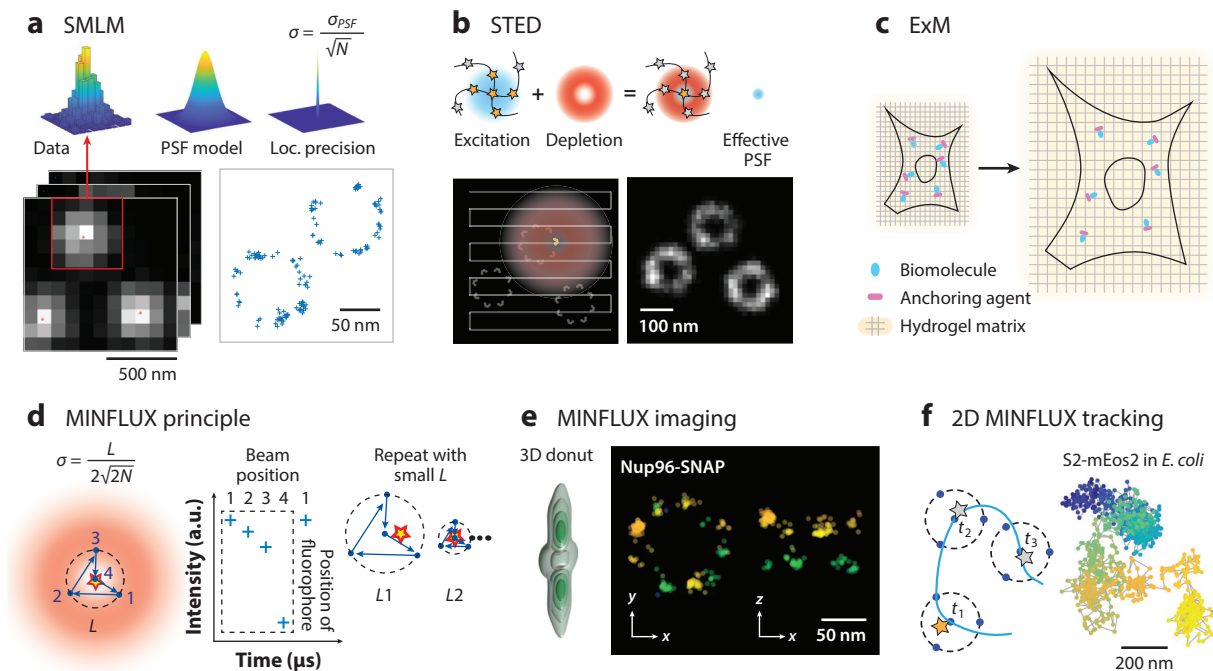


Figure 1

Principle of main super-resolution microscopy (SRM) techniques. (a) Single-molecule localization microscopy (SMLM). Isolated emitters are identified and cropped in small subregions (red box) and fitted with a point spread function (PSF) model; the localization (Loc.) precision σ depends on the number of detected photons N . The emitters' positions are output as coordinates (blue crosses). (b) Stimulated emission depletion (STED). With a donut-shaped depletion beam, fluorescence emission at the periphery of the excitation beam is suppressed, reducing the size of the effective PSF. The excitation beam, together with the depletion beam, raster scans across the field of view to obtain the super-resolution image. (c) Expansion microscopy (ExM). Biomolecules are covalently attached to an anchoring agent that can bind to a swellable hydrogel. After the hydrogel is immersed in water, it will expand the biological specimen by 4–10 times. (d) Principle of MINFLUX (minimal photon flux). A single emitter is probed by a donut beam in a specific scanning pattern, such as a triangular pattern with four positions. The detected photons from those scanning positions are used to estimate the fluorophore's position. As the localization precision σ for MINFLUX is proportional to the scanning pattern size L and depends on the photon count N , the scanning pattern size is iteratively decreased and centered on the fluorophore to achieve better localization precision. (e) 3D MINFLUX imaging of Nup96-SNAP labeled with AF647 in U2OS cells. A 3D donut probes the emitter in an octahedral pattern to estimate its position in three dimensions. Panel e made using data from References 49 and 112. (f) 2D MINFLUX tracking of a single 30S ribosomal subunit protein (S2) tagged with mEos2 in living *Escherichia coli*. The scanning pattern continuously follows the emitter to obtain its positions in time. Panel f adapted with permission from Reference 6. Simulated structures for SMLM and STED are based on the positions of Nup96 proteins in the nuclear pore complex, with a labeling efficiency of 60%.

Point spread function (PSF):

the image of a point-like emitter formed by a microscope; its size determines the resolution of the imaging system

MINFLUX (minimal photon flux):

combines single-molecule detection and donut-shaped excitation to enhance the localization precision

Expansion microscopy (ExM):

expands a fixed biological specimen by attaching proteins of interest with an anchoring agent to a swellable hydrogel

of the depletion beam remain fluorescent, thereby reducing the effective size of the point spread function (PSF). Current STED techniques achieve a resolution down to 20 nm (135), limited by residual laser intensities in the center of the donut-shaped depletion beam and increased photobleaching at the high powers of the depletion laser. In contrast, SMLM pushes the resolution down to a few nanometers, making it a popular method for structural biology. SMLM uses wide-field illumination in combination with fluorophores that are stochastically switched between a long-lived dark off-state and a bright on-state. By activating only a small subset of fluorophores in each camera frame, the well-isolated emitters can be localized with a precision of a few nanometers (**Figure 1a**). High-resolution images are then reconstructed by accumulating thousands to millions of individual localizations. By analyzing not only the position of the single fluorophores, but also the shape of their PSFs, fluorophores can be localized in 3D (60), and the use of spectrally different fluorophores or sequential imaging allows the probing of relative positions of proteins with multicolor SMLM (18, 71, 118).

In SMLM, the number of photons detected from each blinking event limits the resolution. By combining single-molecule detection as in SMLM with structured, donut-shaped excitation similar to STED, this limitation can be overcome. This technique, called MINFLUX (minimal photon flux), can thus considerably improve the resolution compared to SMLM even for dim fluorophores and has a high potential for dynamic SRM with structural resolution.

An alternative strategy for improving the resolution of the microscope is to increase the size of the sample itself. In expansion microscopy (ExM) (**Figure 1c**), the biological sample is fixed and embedded in a hydrogel matrix, which is then expanded by a factor of 4–10 by hydration (143). Thus, even with a standard confocal microscope, structures smaller than 100 nanometers can easily be resolved. In combination with SMLM (ExSMLM), the resolution is improved by the expansion factor (154). Furthermore, combining iterative ExM with labeling of all proteinaceous cellular content (pan-ExM) results in EM-like contrast at high resolution (93). However, due to the sample preparation protocol, which includes polymerization, digestion, and expansion, ExM is not live cell compatible and can distort the biological structure as a result of nonisotropic expansion (129).

In the remainder of this review, we focus on SMLM and its new cousin MINFLUX as the optical microscopy methods with the highest resolution.

Single-Molecule Localization Microscopy

As described above, SMLM relies on imaging a small subset of all emitters in a single camera frame. This is achieved by using fluorophores that transition between a dark and a bright state. The switching mechanism in SMLM is sometimes indicated by the use of different terms. Photoactivated localization microscopy (PALM) (13) and fluorescence photoactivation localization microscopy (FPALM) (53) use photoconvertible or photoactivatable fluorescent proteins. The transition is induced by low intensities of UV laser, and off-switching occurs via photobleaching (13). The use of these genetically encoded fluorophores, without the need for additional labeling steps, special buffers, or fixation is beneficial for quantitative and live-cell SMLM, especially in combination with complete labeling of endogenous proteins. Stochastic optical reconstruction microscopy (STORM) (110) uses a pair of synthetic dyes (e.g., the activator Cy3 and the reporter Cy5) in close proximity in an oxygen-depleted blinking buffer containing a thiol. Exciting the activator with a green laser leads to the switching of the reporter from a dark state to a red fluorescent state. Many synthetic dyes show a similar switching behavior in a blinking buffer under UV illumination, even without activator dyes. This approach, sometimes called dSTORM (52), is the most common approach to SMLM with organic dyes. All of these approaches are conceptually the same and are typically summarized under the term SMLM (for detailed reviews, see 82, 92).

In addition to photoswitching, blinking can be generated through transient binding of freely diffusing fluorophores to the target protein, such as in point accumulation for imaging in nanoscale topography (PAINT) (115) and DNA-PAINT (113). In DNA-PAINT, a short single-stranded DNA molecule (docking strand) is attached to the target protein, and the complementary DNA strands labeled with a dye (imager strand) diffuse freely in the buffer. The imager strands, upon binding to the docking strand, are immobilized and generate a fluorescent on-switching event. Because of the high number of detected photons per binding event, exceptionally high localization precisions of <2 nm can be routinely reached. As the binding by the imaging strand is reversible, different target structures can be imaged sequentially with different imager strands labeled with the same fluorophore for highly multiplexed SMLM (71).

Data analysis is a major part of the SMLM workflow. The most important step is to localize single fluorophores with subpixel accuracy. Typically, this step includes emitter identification, segmentation, and fitting with either a theoretical or an experimentally calibrated PSF model. The positions of the emitters are returned as a list of coordinates. Subsequent data analysis includes postprocessing such as drift correction, rendering of the super-resolution image, and quantitative analysis of biological structures (146).

MINFLUX

The novel super-resolution technique MINFLUX improves the localization precision by probing the emitter with the local minimum of a structured illumination pattern (6, 37, 49, 112). The central minimum of a donut-shaped beam is scanned around the single emitter following a predefined scanning pattern (**Figure 1d**). The photon values detected at all scanning positions, together with the knowledge of the scanning pattern, allow one to extract the emitter's position with a higher precision compared to SMLM for a given number of detected photons. Iteratively moving the central minimum closer to the emitter and, at the same time, shrinking the scanning radius further improves the precision and enables nanometer localization precisions with a small number of detected photons (49, 112) (**Figure 1d,e**). A larger field of view (FoV) can be probed by performing MINFLUX measurements iteratively on a grid (49). In contrast to SMLM, where activation of single fluorophores is stochastic, in MINFLUX, the activation is better controlled: As long as no fluorophore is detected, UV activation is used at high intensities, but upon detection of a fluorophore activation event, the UV laser is switched off. This increases the activation rate and leads to a potentially high imaging speed for small (approximately 100 nm) FoVs.

Since MINFLUX is the most efficient known way of using photons for localization, it is particularly beneficial for high-resolution live-cell imaging with genetically encoded photoconvertible fluorescent proteins, where the photon budget is low. Gwosch et al. (49) demonstrated MINFLUX imaging of Nup96 proteins tagged with mMaple in live cells at 2 nm localization precision. However, the imaging speed of current MINFLUX implementations [approximately 2 min for one nuclear pore complex (NPC) (49)] is too slow for most dynamic processes in living cells. Higher imaging speeds should become feasible with increased excitation laser powers (but at the price of stronger photobleaching and phototoxicity) and with optimized switching schemes that deterministically switch off a fluorophore once it has been localized with sufficient precision.

Time-lapse imaging (i.e., making movies of molecular machines) requires imaging the same fluorophore many times. Currently, however, we lack suitable live cell-compatible photoactivatable fluorophores with many switching cycles. Thus, fulfilling this dream of dynamic structural biology in the cell will depend on future developments of high-speed MINFLUX, including fluorophore engineering; improved optics, electronics, and software; and optimization of imaging and sample preparation conditions.

Point accumulation for imaging in nanoscale topography (PAINT): SMLM variant where transient binding of a fluorophore to the target protein creates a single-molecule activation event

Localization precision: a measure for the uncertainty of the coordinate estimates; depends on detected photons and background

Molecular machines: an assembly of a distinct number of molecular components that undergo functional conformational changes

Besides acquiring super-resolution images with unprecedented resolution in living and fixed cells, MINFLUX also enables single-molecule tracking with high spatial–temporal resolution (Figure 1f). In the so-called tracking mode, the donut beam continuously follows the emitter with a localization rate up to the scanning cycle rate of approximately 10 kHz (37). Since the tracking mode requires no photoswitching, bright fluorophores with a large photon budget can be used, leading to second-long tracks with submillisecond temporal resolution and 2 nm localization precision (37).

Although MINFLUX is a technology that localizes single molecules, there is no consensus on whether it should be considered an SMLM variant. However, as the requirements (single photoactivatable fluorophores) and the output data (position estimates of these fluorophores) are similar to SMLM, most of the following discussion of SMLM is also valid for MINFLUX.

PUSHING SINGLE-MOLECULE LOCALIZATION MICROSCOPY TOWARD STRUCTURAL SCALES

What does structural resolution mean for SMLM measurements? In contrast to classical structural biology methods, optical methods will never measure the structure of an entire protein; the best that they can do is to determine the precise positions of a few epitopes, labeled with fluorophores. However, these positions can tell us a lot about the conformation of a protein in the cell and about how individual proteins are arranged in a complex, especially if we take into account structures determined with classical techniques. The ultimate resolution in SRM is determined by the size of the label and is thus on the order of 1 nm. However, reaching such a high resolution is challenging and requires powerful and ultrastable microscopes, bright fluorophores, and labeling approaches that only minimally displace the fluorophore from the epitope. In addition, structural insights are often based on the relative positions of epitopes, determination of which requires multicolor SRM. Often, not only the relative arrangement of proteins, but also their copy number in a complex, is highly important to understanding the structure and function of a molecular machine. Dynamic measurements in living cells are still especially challenging but necessary to make use of this key advantage of SRM compared to classical structural techniques. Finally, extracting biological insights from SMLM data in a statistically meaningful way requires not only large data sets that are limited by the slow speed of SMLM, but also new data analysis approaches. In the following sections, we discuss how new developments of SMLM were able to overcome these challenges.

New Microscopes to Reach Nanometer 3D Resolution

One major extension of SMLM was to measure 3D positions of single fluorophores by evaluating the shape of the PSF. The 3D resolution was then further improved by new microscopes that use interference, detect near-field fluorescence, or excite the sample with structured light. To reach their potential, these microscopes need to be stable on the single-nanometer scale.

Point spread function–based 3D single-molecule localization microscopy. Standard localization algorithms extract x and y positions of single isolated fluorophores from camera images but do not provide any information about the fluorophore's z position. This is a big limitation, as biological structures are intrinsically 3D. A solution is to evaluate not only the position of the fluorophore image, but also its shape. For the shape to carry sufficient information about the z position, distortion of the PSF, in an approach called PSF engineering, or viewing the PSF at two or more z positions in bi- or multiplane SMLM is usually required. The most simple and common approach to 3D SMLM is to induce astigmatism in the detection beam path with a cylindrical lens (60); the aspect ratio of the now elliptical PSF will then provide information on the z position

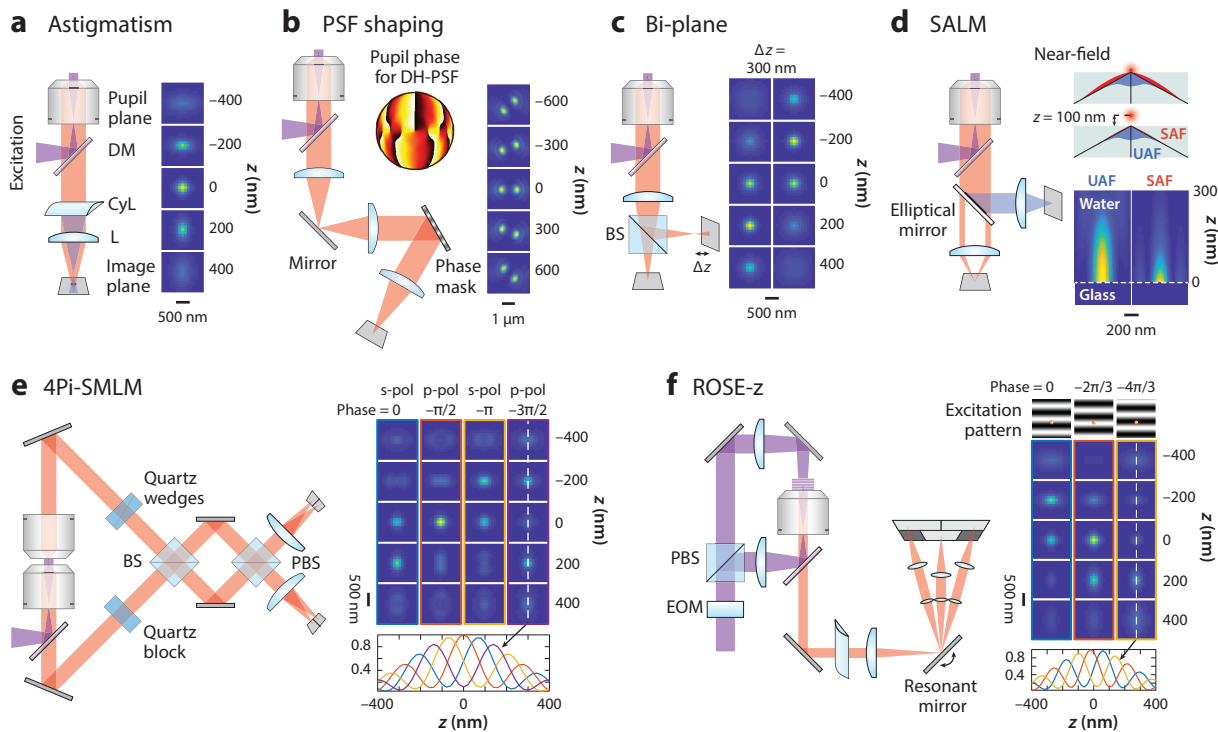


Figure 2

Principle of 3D single-molecule localization microscopy (SMLM) techniques. (a) Astigmatism. Astigmatism is introduced by adding a cylindrical lens (CyL) in the imaging path; the shape of the point spread function (PSF) then encodes the z position. L denotes a spherical lens, and DM denotes a dichroic mirror. (b) PSF engineering techniques. A phase mask is added at the Fourier plane of the imaging path to encode the z information in the PSF patterns. The example shows the double-helix PSF (DH-PSF) and the corresponding phase mask. (c) Bi-plane method. The emission path is split into two channels, with one channel defocused by Δz . This additional channel breaks the symmetry along the axial dimension, improving the localization precision, especially at z positions around the focus. (d) Supercritical angle localization microscopy (SALM). The near-field emission of a fluorophore close to the glass–water interface propagates at an angle above the critical angle (red shaded area in the polar plots of dipole radiation). In SALM, the undercritical fluorescence (UAF) is reflected by an ellipse-shaped reflection surface coated on a glass window, while the supercritical angle fluorescence (SAF) is transmitted through the glass window. As the SAF decays quickly with the distance of the fluorophore from the interface, the ratio of SAF to UAF provides a precise and absolute measure for the fluorophore's z position. Panel *d* adapted with permission from Reference 30. (e) 4Pi-SMLM. Fluorescence collected by two objectives is combined and interferes at the beam splitter (BS). The interference signals are separated into four channels with s- and p-polarizations (s-pol and p-pol) after a polarized BS (PBS). The phase separation between the four channels is set to approximately $\pi/2$ by adjusting the thickness of the quartz wedges. The intensity at the PSF center is modulated along the axial dimension at a period close to half of the emission wavelength. The strong modulation of the signal in z gives rise to a high z resolution. (f) Repetitive optical selective exposure (ROSE)- z as an example of modulation-enhanced SMLM. A standing wave along the axial dimension is generated from the interference of two laser beams. The resonant mirror distributes the fluorescence emissions with high speed at three excitation patterns whose phases are separated by $2\pi/3$ into three detection channels. The excitation pattern is switched by an electro-optical modulator (EOM), which is synchronized with the resonant mirror. Similar to 4Pi-SMLM, the intensity at the PSF center is modulated along the axial dimension with a modulation period equal to the period of the standing wave.

(Figure 2a). Due to its simplicity and stability, astigmatism imaging has been used to resolve the structural organization of multiprotein machineries, such as the NPC (67) or the centriole (120). Other PSF engineering techniques, such as double-helix (101) (Figure 2b), tetrapod (116), and self-interference (16) PSFs, have been developed for either extended axial range or

Modulation-enhanced localization microscopy (meLM): combines modulated wide-field illumination patterns with single-molecule detection to enhance the localization precision

higher tolerance to aberrations. Bi- or multiplane SMLM (50, 69) simultaneously images single fluorophores at two or more focal planes and extracts z positions from the size of these partially defocused single-fluorophore images (**Figure 2c**). All of these approaches require a calibration of the PSF, which is usually achieved by acquiring a z -stack of fluorescent beads immobilized on the coverslip. A realistic, experimentally derived model for the PSF during fitting, in contrast to a Gaussian approximation, improves the precision and reduces systematic errors in z (83).

4Pi-single-molecule localization microscopy. The highest z resolution in SMLM can be achieved with interferometric detection methods, such as iPALM (119), 4Pi-SMS (3), and W-4PiSMSN (63). In these methods, referred to as 4Pi-SMLM, the sample is sandwiched between two objectives, and the fluorescence of single fluorophores collected by the two opposing objectives is interfered on a beam splitter (**Figure 2e**). The z position of the fluorophore determines the path difference between the two interferometer arms, leading to constructive or destructive interference. The central intensity of the 4Pi-PSFs is thus modulated with the emitter's axial position at a period of approximately $\lambda/2$. The twofold increase in collected photons, combined with this strong intensity modulation, results in a 5–7-fold increase in the axial resolution compared to single-objective SMLM, while the complex features of the 4Pi-PSFs in the lateral dimension provide 1.4–2-fold lateral resolution improvement. Interferometric detection is especially sensitive to instabilities; thus, it is challenging to reach the theoretical resolution. Imaging in thick samples requires index matching and the use of a silicon oil objective (140) to avoid loss in modulation contrast (85).

Modulation-enhanced localization microscopy. Inspired by MINFLUX, several SMLM techniques combine modulated illumination patterns with single-molecule detection to improve the localization precision; these techniques include SIMFLUX (26), repetitive optical selective exposure (ROSE) (47), ROSE- z (48), ModLoc (68), and SIMPLE (106). In those methods, sometimes referred to as modulation-enhanced localization microscopy (meLM) (105), single emitters are scanned by sinusoidal illumination patterns at different phases and orientations, and the resulting intensity-modulated images are used for position estimation. Typically, these approaches can double the resolution for a given number of detected photons compared to standard SMLM. In this section, we focus on discussing ROSE and ROSE- z , which outperform the other techniques.

ROSE utilizes fast pattern switching and simultaneous readout of images from all illumination patterns within one camera exposure. In this method, illumination patterns can be switched at kHz rate by using electro-optical modulators, and signals from all illumination patterns are sequentially projected onto the subregions of the detection cameras with a resonant mirror. Hundreds of scanning cycles are averaged during one camera exposure, resulting in quasisimultaneous detection, which eliminates localization errors caused by fluorescence blinking.

ROSE- z applies this scanning technique in the axial dimension by scanning the emitters with a standing wave generated from two counter-propagating laser beams, improving the axial resolution by sixfold (**Figure 2f**). In comparison to 4Pi-SMLM, ROSE- z improves only the axial resolution and collects half of the emitted photons from single-objective detection; therefore, the theoretical resolution of ROSE- z is lower than that for 4Pi-SMLM. In practice, however, ROSE- z achieves performance comparable to that of 4Pi-SMLM but with a much simpler and more robust setup. The reason for this is that interference of coherent laser beams in ROSE- z is depth independent, is more robust, and creates a higher modulation contrast than interference of incoherent fluorescent light in 4Pi-SMLM. Additionally, 4Pi-SMLM is more sensitive to drifts between the objectives and contains a large number of optical components in the beam path, which causes a loss in detected photons.

Supercritical angle fluorescence. For high numerical aperture (NA) objectives ($NA > 1.49$), the evanescent wave from a fluorophore's dipole emission couples through the water–glass interface directly into the glass. This effect is termed supercritical angle fluorescence (SAF) (109). This extra emission, which appears at angles above the critical angle (the angle above which total internal reflection occurs), decays quickly with the distance of the emitter from the coverslip and offers a sensitive measure of the emitter's z position. Supercritical angle localization microscopy (SALM) (32) and direct optical nanoscopy with axially localized detection (19) have been used to apply SAF to SMLM (**Figure 2d**) and achieved a resolution of approximately 8 nm in all three dimensions (30). However, SAF only occurs within a few hundred nanometers, limiting this technique to the vicinity of the coverslip.

Stability

The high resolution and long data acquisition time in SMLM lead to exceptional requirements for the stability of the microscopes. Drift and vibrations become major factors that limit the achievable resolution.

Vibrations are oscillations of microscope components that lead to rapid displacements of the image. In contrast to slow drift, fast vibrations are very difficult to counteract with active stabilization or to correct in a postprocessing step. Although they are rarely evaluated for SMLM systems, these vibrations regularly make up a main limitation in resolution, especially for high-resolution techniques such as DNA-PAINT or MINFLUX.

Proper design of the microscopes and their decoupling from the environment can reduce vibrations. By adjusting the frame rate to the main vibration frequency, high-frequency vibrations (> 50 Hz) can partially be averaged out in SMLM. Low-frequency vibrations are often negligible (64) or can be compensated by active drift correction. Fast SMLM (61) or MINFLUX (37) can operate at a localization rate of 1–10 kHz, requiring a full evaluation and optimization of the vibrations.

Mechanical drift exists for all SMLM systems and is often caused by small temperature changes. It can be categorized into sample-stage drift and system drift.

Sample-stage drift includes the drift that occurs at the sample, sample stage, and objectives. Lateral drift is often corrected during postprocessing, but the focal position should be actively stabilized, as z drift can lead to a nonuniform lateral drift caused by field-dependent aberrations. Commercial (e.g., Nikon Perfect Focus and Zeiss Definite Focus) or custom (<http://big.umassmed.edu/wiki/index.php>) focus-locking methods are often based on detecting the position of an infrared laser reflected at the coverslip and can reach precisions of 20 to 30 nm (28). Active 3D drift correction methods use bright fluorophores or fluorescence beads (102), bright-field images of the sample itself (90), micron-sized polystyrene microspheres (27), or the back-scattered laser light of gold nanorods (112) and achieve a stabilization precision down to 1 nm in all three dimensions.

System drift includes the drift that occurs within the detection path after the objectives. A micron-sized pinhole illuminated by a white LED can be used as an optical fiducial to account for system drift between two detection channels (27, 102).

Interference phase drift is specific to systems using interferometric detection or illumination, such as in 4Pi-SMLM (85) and ROSE- z (48). Interference phase drifts are mainly caused by temperature fluctuations and air flow. As the z position is extracted from the interference phase, phase drift can lead to an effective z position drift of a few hundred nanometers. This can be reduced by enclosures and temperature-controlled environments (140) or corrected during postprocessing (48, 63).

Supercritical angle fluorescence (SAF): fluorescence emission that appears at angles above the critical angle; decays exponentially with the distance from the emitter to the coverslip

Field-dependent aberration: variation of the PSF that depends on the position of the emitter within the field of view

Beam drift is specific to MINFLUX systems, where the position estimation relies on the shape and the position of the excitation beam.

Fiducial marker:

an object that can be imaged with high contrast, used for drift correction or image registration

Labeling efficiency:

the fraction of target proteins that carry a fluorophore that can be detected during imaging

Drift correction during postprocessing is usually required for high-resolution SMLM. Even with active stabilization, residual drift remains. It can be estimated and corrected during postprocessing either from the positions of fiducial markers (5, 15, 72, 120) or from the single-molecule data themselves (91, 142). Redundant cross-correlation (RCC) (142) divides the data into segments of equal time and computes the image cross-correlation between all pairs of data segments to obtain an estimation of the drift over time. As each data segment requires a sufficient number of localizations in defined structures, RCC is best suited to correcting for long-term drift. RCC can also be used to correct drift with the help of fiducial markers, as these create a strong cross-correlation signal. Drift at minimum entropy estimates the drift by maximizing the sharpness of the resulting images and achieves a precision comparable to that of fiducial markers with a small data segment size (approximately 50 frames) (25).

Improved Labels for Single-Molecule Localization Microscopy

Structural SMLM aims to measure precise positions of biomolecules. This requires a high labeling efficiency, i.e., that most of the target molecules are labeled with a fluorophore. As the localization precision in SMLM depends directly on the detected number of photons, bright fluorophores are indispensable when pushing the resolution of SMLM to structural scales. The attainable resolution is then limited by the size of the labels. In the following sections, we discuss how the choice of fluorophores and labeling approaches enables high-resolution SMLM.

Fluorophore brightness. During SMLM imaging, fluorophores are switched on and off stochastically, and the number of photons collected during each on-time of the fluorophore determines the localization precision. The interplay among fluorophore brightness, off-switching kinetics, and photobleaching determines the total photon count per emission event. Synthetic organic fluorophores can be one order of magnitude brighter than fluorescent proteins (141) and are often more photostable but require either a special thiol-containing blinking buffer or a photocleavable group. Fluorophore brightness can be increased by replacing normal water with heavy water (75, 80, 98) and by optimizing buffer conditions (31, 34). DNA-PAINT (71) circumvents the problem of photoswitching by generating blinking through transient binding of the fluorophore to the target protein. As no additional blinking needs to be induced, the fluorophores can emit their entire photon budget during a single binding event, resulting in a 10–20-fold increase in photon count compared to dSTORM.

Photostability is another crucial factor to achieve high photon counts. Oxygen scavenger systems can reduce photobleaching (12), but resulting long-lived triplet states need to be quenched (97, 138).

Achieving high photon yield in live-cell imaging is still challenging (38, 141). First, most organic fluorophores are cell impermeable; thus, the development of bright and cell-permeable fluorophores, such as PA-JF dyes (45, 46), is important. Second, many photostabilization agents and reactivation with UV are toxic to live cells. Self-healing dyes constructed from conjugating organic fluorophores with photostabilizers [e.g., COT-Cy5 (1)] can effectively stabilize the fluorophore without adding photostabilizing agents to the imaging buffer (66). Self-blinking dyes have the advantage that they demonstrate SMLM-compatible switching without the need for UV activation or special buffer conditions, but this approach lacks the flexibility of easily adjusting the activation rate (79, 126, 132). In general, membrane-permeable photocaged or self-blinking dyes and photoswitchable fluorescence proteins are still the best choices for live-cell SMLM.

Size of the label and linkage errors. As the localization precision of SMLM techniques continuously improves, it becomes increasingly important to reduce the labeling size to further enhance the achievable image resolution (**Figure 3**). Commonly used immunofluorescent labeling methods with primary and secondary antibodies will displace fluorophore targets by up to 20 nm from the protein due to the large size of the antibody (10–15 nm, 150 kDa); even when the fluorophores are directly conjugated to the primary antibody, labeling will still cause up to 13 nm linkage error (40). Fusing the target protein with photoswitchable fluorescence proteins, such as mEos3.2 (150) or mMaple (89), or self-labeling enzymes, such as SNAP- (73), Halo- (86), or CLIP-tag (42), reduces the linkage error to 2–3 nm. However, the relatively large

Linkage error: displacement of the fluorophore from the epitope or tagging site of the target protein

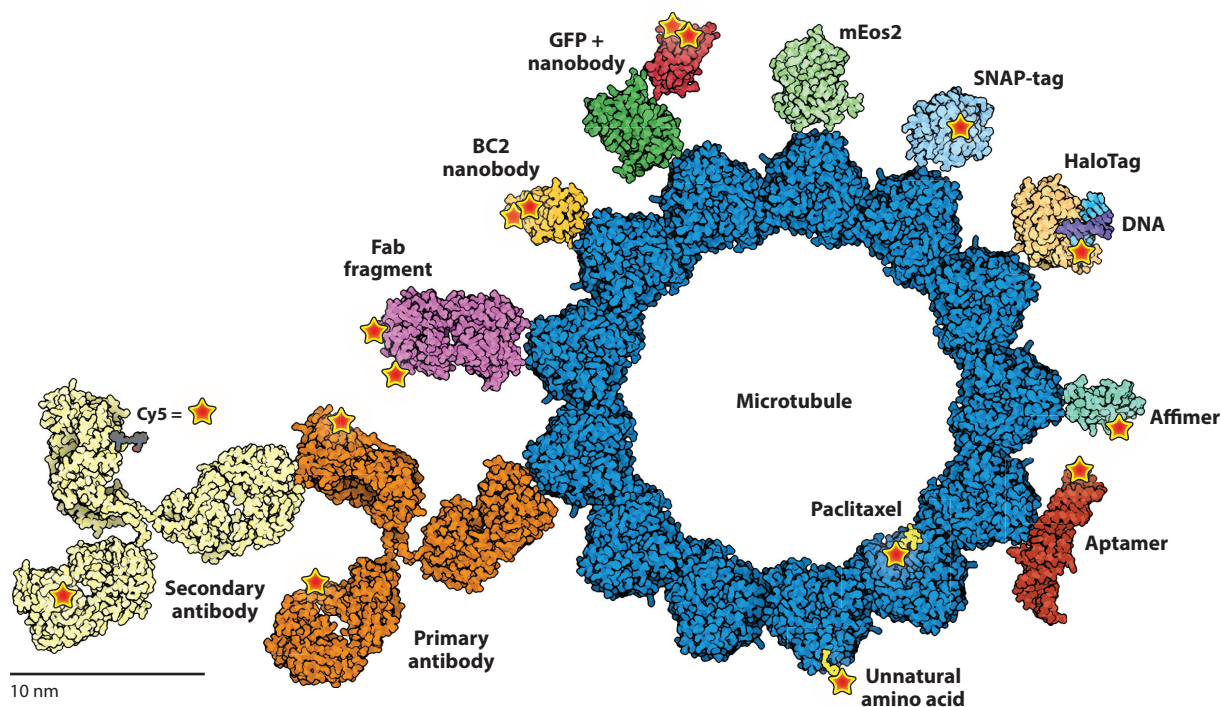


Figure 3

Different labeling techniques for SMLM. The structure of interest [in this case, a microtubule; β -tubulin (PDB ID 5SYF) is shown in dark blue on top] can be labeled in different ways: The classical immunolabeling with primary (orange; PDB ID 11GT) and secondary (light yellow) antibodies is commonly used but introduces a large linkage error. To overcome this, smaller proteins can be used that bind specifically to the target structure, such as Fab fragments (purple; PDB ID 3QNZ) and nanobodies binding to epitope tags or the native protein (yellow; PDB ID 5IVN) or GFP (green, nanobody in red; PDB ID 3OGO). An alternative is to use photoswitchable fluorescent proteins like those of the mEos family (light green; PDB ID 3S05). The use of self-labeling enzyme tags like SNAP-tag (light blue; PDB ID 3KZY) or HaloTag (yellow; PDB ID 6Y7A) allows labeling with synthetic dyes or single-stranded DNA for DNA-PAINT (eight base pairs shown in purple and turquoise attached to the HaloTag; PDB ID 1BNA). Affimers are non-antibody-derived proteins that also specifically bind to a target structure (light green; PDB ID 4N6T), similar to RNA-based aptamers (dark red; PDB ID 5OB3). Furthermore, small molecules that specifically bind to certain proteins can be used for SMLM, such as paclitaxel binding to β -tubulin (yellow, displayed on top instead of buried within the protein for visualization; PDB ID 5SYF). Introduction of an unnatural amino acid (in this case, cyclooctene-*L*-lysine) into the target protein allows SMLM with minimal linkage error (yellow; PDB ID 6AAO). The respective structures were downloaded from the PDB and rendered using Illustrate (43). Abbreviations: PAINT, point accumulation for imaging in nanoscale topography; PDB, Protein Data Bank; SMLM, single-molecule localization microscopy.

Chromatic

aberration: distortion of the emitter's apparent position that depends on the wavelength of the emitted fluorescence

proteins and enzymes (20–30 kDa) may influence the function of the target protein (136, 141). Alternative choices include Fab fragments (antigen-binding domains of regular immunoglobulin G antibodies) or nanobodies (single-domain antibodies, 15 kDa, 2 nm) to directly label the native protein target (130), GFP fusion proteins (107), or short and inert peptide tags [BC2- or spot-tag, 1.4 kDa (136); ALFA tag, 1.9 kDa (44)].

Non-antibody molecules that bind specifically to target proteins, such as aptamers [single-stranded DNA or RNA oligonucleotides, 13–15 kDa (99)] or affimers [polypeptide, 10–12 kDa (23, 111)], have been recently applied to SMLM imaging and can be easily purified in large quantities. Another alternative is to use small molecules that are derived from natural toxins, such as paclitaxel (taxol), which stains microtubules (7), or phalloidin, which binds to filamentous actin (147).

To further minimize the linkage error, as well as the disruption of the protein function, site-specific labeling, by incorporating a single unnatural amino acid into the target protein and labeling it with bright organic fluorophores by click chemistry, has been recently demonstrated for SMLM imaging (11, 133).

Multicolor Single-Molecule Localization Microscopy

Investigating the spatial relationship among different proteins requires multicolor SMLM, which can be realized by different approaches extending standard SMLM. Important points to consider when choosing an approach are compatibility of the fluorophores in the specific imaging buffer, decreased resolution compared to single-color measurements, registration of the channels, and chromatic aberrations. The most straightforward implementation is to sequentially image the channels with the same fluorophores, either using different activators in the STORM approach (9) or by repeated cycles of staining, imaging, bleaching, and restaining (127, 134). In DNA-PAINT, it is possible to label different structures with distinct docking strands, which are sequentially visualized by supplying different imager strands with the same fluorophore (71). Green-to-red photoconvertible fluorescent proteins like mMaple or mEos are typically converted by UV activation, but some can also be converted by exciting them with a green laser and then illuminating the excited state with a far-red (730 nm) laser (131). This so-called primed conversion allows one to perform sequential acquisitions of primed-convertible and standard UV-convertible fluorescent proteins in the near-red channel (137). The advantages of these sequential approaches are that, due to the use of the same fluorophore, there are no chromatic aberrations, registration of the channels is not necessary, and the image quality is the same as for single-color experiments. However, fiducial markers or additional bright-field images are necessary to correct for drift.

Spectrally different fluorophores can be split in the emission path of the microscope and detected separately. Examples for this are Cy5/rsFastLime (14), Dronpa/tdEos (118), AF647/AF750 (152), and AF647/mMaple (56, 94). In this setting, a transformation between the two channels has to be determined to allow their overlaying.

Another approach is to use spectrally similar but not identical fluorophores in combination with ratiometric detection. This means that the emitted fluorescence is split into two channels within the range of these fluorophores' emission maxima, and therefore, the intensity is split in ratios characteristic for a particular dye. Analysis of these ratios during postprocessing allows one to reassign a color to individual localizations, and the transformation between the channels can be determined from the data themselves, as the single fluorophores are localized in both channels. In this way, three (18) or even four (128) fluorophores can be distinguished. The disadvantage of lowered localization precision due to a decrease in the number of photons by splitting of the signal was recently resolved by using the emitted fluorescence that gets reflected at the microscope's main dichroic mirror to assign colors to individual localizations (151).

Speed and Throughput

Using SMLM for structural studies of molecular machines, for example, by averaging or dynamic reconstruction, requires large amounts of data. As acquisitions in SMLM take a long time, several efforts were made to increase the throughput and speed up the imaging procedure. Automated SMLM imaging without user intervention results in high throughput (10, 58, 94). Another strategy is to increase the FoV to image more structures of interest at the same time. This was enabled by stronger lasers, the use of scientific complementary metal oxide semiconductor (sCMOS) cameras for SMLM (61), and new homogenous illumination schemes (33, 35, 124).

The imaging speed of SMLM can be increased by switching the fluorophores faster using stronger lasers (8, 84), but this comes at the price of decreased image quality caused by loss of fluorophores and reduced photon counts due to increased photobleaching at high intensities (34). Finally, acquisition speeds can be increased by activating fluorophores to higher densities beyond the single-molecule regime to a point where the PSFs of individual emitters overlap. This requires multi-emitter fitting algorithms (4, 59, 62, 153). Deep learning-based high-density fitters (95, 123) showed an improved robustness and precision compared to traditional fitting approaches.

Dynamic Live-Cell Imaging

Ideally, in situ structural biology of molecular machines would be performed in living cells to enable analysis of dynamic structural changes. However, in SMLM, high laser powers are necessary to induce single-molecule blinking and to localize single fluorophores with high precision, which often entails phototoxicity. Thus, proper controls are indispensable to ensure that the structure and dynamics of the process under investigation are not altered by the imaging process. Activating fluorophores to high densities in combination with proper multi-emitter fitters increases the number of localizations for a given light exposure (123) and provides an opportunity to match the rather slow imaging of SMLM to the potentially fast biological process under investigation.

In addition to the low photon yield of live cell-compatible fluorophores (as discussed above), many of these fluorophores are activated only once and switch off irreversibly by photobleaching. Thus, they are visible only in one or a few images of a time-lapse movie, resulting in poor effective labeling efficiencies and making dynamic changes difficult to observe. These disadvantages make it desirable to develop fluorophores that are live cell compatible, i.e., are membrane permeable, blink under physiological conditions, and can be reactivated multiple times.

If live-cell imaging of a molecular machine is not feasible, then an alternative approach is to reconstruct structure and dynamics from a large number of fixed snapshots (see below).

Counting of Proteins

As SMLM contains not only spatial but also quantitative information about the fluorophores, such as the number of localizations and the blinking kinetics, it can be used to count individual fluorophores. There are several pitfalls that have to be considered when calculating absolute protein numbers from individual blinking events: Flickering and reactivation of the fluorophore leads to overcounting, whereas bleaching, misfolding of the protein tag, delayed fluorophore maturation, and overactivation that leads to rejection of overlapping localization events result in undercounting. In general, photoconvertible fluorescent proteins or photoactivatable synthetic dyes are advantageous for quantitative SMLM, as their blinking behavior is more regular compared to synthetic dyes like AF647, which go through several switching cycles.

Given that, rather than the number of fluorophores, the number of proteins is usually the factor of interest, achieving reproducible and quantitative labeling of the target structures is a

Dynamic reconstruction: extracting dynamic information from static snapshots to sort them in time and align them in space

Endogenous and homozygous labeling:

editing all alleles in the genome of the investigated organism to have a 1:1 stoichiometry of target protein and label

major challenge; the highest counting accuracies can be achieved by endogenous and homozygous labeling of the target proteins with photoconvertible fluorescent proteins (129).

One way of relating the counted localizations to an absolute protein copy number is to calibrate the blinking by modeling the transitions between different fluorophore states (bright and dark states). This has been done for the photophysics of fluorescent proteins (2, 36, 81, 108) and synthetic dyes such as AF647 (96). This analysis can be facilitated by using DNA-PAINT because the blinking is not caused by photophysics but is instead the result of DNA binding kinetics (70). However, all of these approaches to model blinking count only the fluorophores and not the proteins and thus suffer from nonstoichiometric labeling. Even for, e.g., homozygous endogenous tagging, incomplete fluorophore maturation and steric hindrances when using external labels lead to a reduced labeling ratio of the target structure and thus undercounting.

Another strategy employed is to use a reference whose stoichiometry is known to determine the calibration factor between observed localizations and copy number. This reference can be composed of multiple repeats of the same fluorescent protein (103), tagged proteins forming homo-oligomers of different size (39), DNA origami (149), or a well-defined intracellular protein complex like the NPC (129).

Data Analysis

A visual inspection of reconstructed super-resolution images is the first step in data analysis, and this step alone can sometimes provide insights into the biology. As a second step, however, quantitative and statistical analyses of the data to investigate hypotheses are indispensable. As the data in SMLM consist of positions of fluorophores, analysis approaches that directly use these coordinates, rather than the reconstructed images, as input are often more efficient and precise, as they can incorporate additional information on localization uncertainties. In the following sections, we briefly discuss different data analysis approaches and refer to a recent review article for an in-depth discussion (146).

Geometric analysis. Geometric analyses are often applied to SMLM data to extract geometric parameters that quantify the biological structure (146), such as distances, diameters, thickness, and periodicity. Distances are often measured through a two-peak Gaussian fitting of a histogram distribution of the localized positions along the measured dimension, such as the diameter of the microtubules (63) or the layered distribution of proteins that compose focal adhesions (72). Given that many molecular machines are circularly symmetric, the radius is another commonly measured geometric parameter, and it can be estimated from fitting a ring model, such as in measuring the radial organization of the proteins in endocytic sites (94), the NPC (67, 125, 129), and cilia (117). Thickness is often extracted together with the distance and radius measurement as the thickness of the ring or the full width half maximum from the Gaussian fitting (72). Periodicity measures the period and the repetition number of a repetitive structure, which is often quantified using linear cross-correlation or directly from the localizations' distribution along a spatial dimension or along the angle. Examples of this analysis include studies of the periodic organization of the actin-spectrin network in axons (148) or of fibronectin in fibrils (41), the eightfold symmetry of NPCs (55, 129), and the ninefold symmetry of the ciliary distal appendage (117).

Quantitative analysis can also be performed by fitting a complex geometric model to the localization data. The model is typically based on prior knowledge (e.g., from EM or other super-resolution studies) and is used to extract measurements that are free parameters during the fitting process (145).

Particle averaging. Averaging of many copies of identical particles is routinely performed in cryo-EM (21, 24, 104) to reconstruct the protein structure. An analog to such techniques has been

recently applied to SMLM, and we refer to these techniques as particle averaging. These approaches aim to calculate average representations with increased labeling densities and contrast from multiple copies of identical biological structures. They can be categorized into pixel-based and coordinate-based methods. The pixel-based methods generate high-resolution particle images by binning the localizations in finite pixels and subsequently aligning the particle images using cross-correlation. This method has been successfully applied to measure the radial and axial organization of the nucleoporins in the NPC with very high precision (67, 125). However, as SMLM imaging produces a list of coordinates, it is natural to directly perform particle averaging on the coordinates' level, where the localization uncertainty can be easily incorporated. Early implementations of coordinate-based methods used a particle template from prior knowledge to align all of the particles with respect to the template (22, 88). However, template-based methods are prone to biasing the resulting structure toward the template and are not applicable to unknown structures. Template-free methods overcome this problem by generating a data-driven template by maximizing a merit function that describes the distance measure (55, 54), the cross-correlation (114), or the probability (145) of pairwise particles. The obtained template is then used to align all of the particles. This procedure can be iterated several times until the averaged particle converges.

Particle averaging: obtaining average distribution maps of proteins and their complexes from many images of identical particles

Dynamic reconstruction. To achieve high spatial resolution, the data acquisition time for SMLM imaging can take several hours, which is too slow to resolve fast dynamic changes of a molecular machine. Thus, samples are often fixed, and the resulting images only show the snapshots of the protein assembly. One method to recover temporal information is to use a timing marker, such as by tagging a reference protein with GFP. If the abundance of the reference protein changes monotonously over time, then the intensity of the GFP signal encodes the time information and can be used to sort the target protein in time (94). Alternatively, a reference structure can be used for dynamic reconstruction by quantifying a parameter of the structure that changes monotonously in time (145). Combining this reference structure with a target protein in the second channel in dual-color SMLM allows the reconstruction of dynamic protein maps. However, these methods require collection of a large number of images of the same protein complex to achieve sufficient sampling at all time points.

Correlative Single-Molecule Localization Microscopy and Electron Microscopy

Correlative SRM and EM (CSREM), combining the two complementary techniques, is able to locate target proteins within its cellular context (74, 51). Early implementation of CSREM correlated EM images from scanning EM, transmission EM, and metal-replica EM with SMLM to study the protein organization in the NPC (87), in the centriole distal appendages (20), and at endocytic sites (122). However, the typical sample preparation for EM undergoes harsh sample treatment, including strong chemical fixation, heavy metal staining, dehydration, and embedding, which will lead to disturbance of the cellular structure and deterioration of the fluorophore performance (51, 77). The emerging techniques that correlate cryogenic electron tomography (cryo-ET) with SRM (SR-cryoCLEM) circumvent all of the harsh sample treatment through cryofixation that preserves both the cellular ultrastructure and the fluorescence and is able to resolve the cellular ultrastructure at atomic resolution without additional staining (29, 57). Furthermore, many fluorescent proteins and organic dyes show a decreased photobleaching rate and an increased photon yield at cryogenic temperatures compared with normal imaging conditions at room temperature, allowing subnanometer precision for sparsely labeled samples (144). However, numerous challenges remain for SR-cryoCLEM, including fluorescent imaging and fluorophore switching behavior at cryogenic conditions, devitrification from optical illumination, and registration between super-resolution and cryo-ET data (29).

APPLICATION OF SUPER-RESOLUTION MICROSCOPY TO STRUCTURAL CELL BIOLOGY

Historically, structural biology solved structures of single proteins or small protein complexes. However, molecular machines typically consist of several subunits, and elucidating their interplay is crucial to understanding their function on a molecular level. Recent progress in EM now allows the analysis of protein complexes as a whole in their native environment and has allowed, for example, the reconstruction of the NPC in its entirety (139). Identification of individual proteins within the electron density requires high resolution, which can only be achieved by averaging multiple identical particles. Analysis of flexible regions of protein complexes or less regular molecular structures is not possible. This gap can be filled by SMLM, as molecular contrast and identity is given by the nature of fluorescence microscopy. In this section, we discuss some examples where SMLM provided insights into the structure of protein assemblies.

An early example for the identification of a new molecular structure by SMLM is the discovery of the periodic membrane skeleton in axons (148) (**Figure 4a**). It consists of circumferential actin rings that are connected by spectrin tetramers, giving rise to a 190 nm periodicity.

The NPC is a molecular machine of approximately 100 MDa that is important for nuclear import and export and has been investigated by SMLM from very early on. Dual-color localization microscopy and averaging of hundreds of NPCs showed the eightfold symmetry and the central channel (88). Furthermore, SMLM in combination with particle averaging allowed researchers to determine radial fluorophore positions with subnanometer precision and therefore to locate the Y-shaped subcomplex within the NPC, whose position was previously ambiguous from EM data (125) (**Figure 4b**). Extension of NPC imaging to three dimensions and the combination of different endogenously tagged subunits with a reference structure in two different colors enabled the visualization of relative positioning for six different proteins: four structural nucleoporins in the cytoplasmic and nucleoplasmic rings, one nucleoporin in the nuclear basket, and one nucleoporin in the largely unstructured cytoplasmic filaments (67). This 3D SMLM approach also allowed investigation of the structural variability among individual NPCs (67).

Clathrin-mediated endocytosis (CME) is carried out by a molecular machine that consists of more than 50 different proteins. For a large subset of these proteins, the average radial distribution in the plane of the plasma membrane has been determined by automated SMLM in endogenously tagged yeast strains from thousands of endocytic sites (94) (**Figure 4c**) and provided novel insights into the assembly process, structural organization, and force generation during the process of CME. In mammalian cells, a combination of platinum replica electron microscopy and SMLM (122) revealed that endocytic proteins are also arranged in distinct spatial zones.

Another cellular structure studied in detail by SMLM is the centriole, a membraneless and microtubule-based organelle that forms the basis for centrosomes, cilia, and flagella (17). Dual-color SMLM was used to localize proteins within the centrosome (121). A recent study combined high-throughput SMLM of purified centrioles and single-particle analysis from single-particle cryo-EM to generate a 3D protein map in four colors by integrating and reconstructing different 2D dual-color data sets (120) (**Figure 4d**).

Additional examples where SMLM resulted in structural insights include studies of the architecture of the cytokinetic ring in living fission yeast (78), the localization and orientation of proteins within the synaptonemal complex in *Caenorhabditis elegans* (65, 76) (**Figure 4e**), and a hypothesized circular arrangement of the MICOS complex at mitochondrial crista junctions by MINFLUX (100).

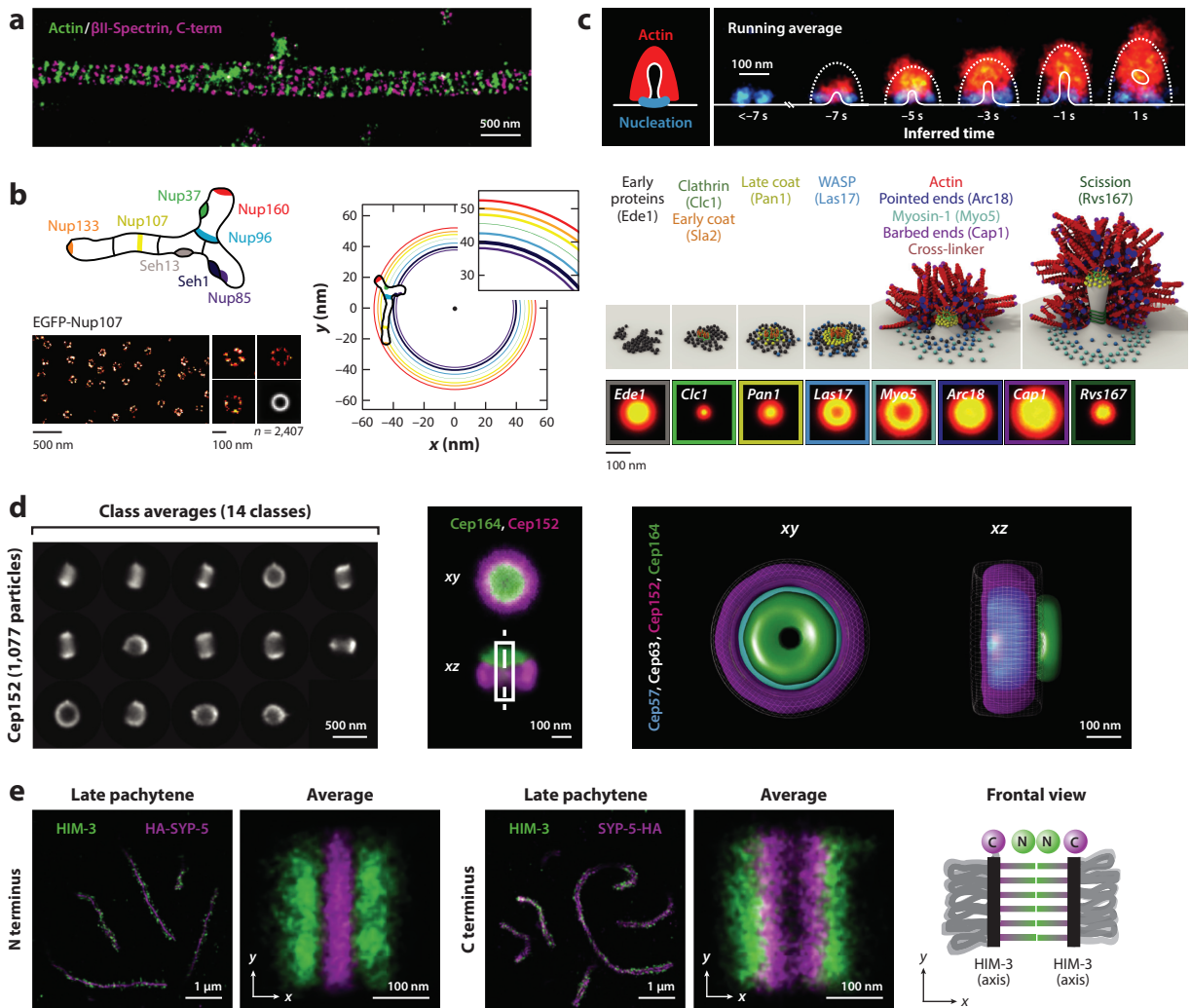


Figure 4

Applications of single-molecule localization microscopy (SMLM) to investigate structures of multiprotein assemblies in cells. (a) The periodic actin–spectrin skeleton in axons was first visualized by SMLM. Panel a adapted with permission from Reference 148. (b) Averaging of hundreds of super-resolved nuclear pore complexes (NPCs) revealed the orientation of the Y-shaped subcomplex within the NPC. Panel b adapted with permission from Reference 125. (c) SMLM of endocytic sites in yeast allowed to resolve the average radial distribution of different proteins comprising the endocytic machinery. Panel c adapted with permission from Reference 94. (d) Using a combination of high-throughput SMLM and single-particle analysis, a 3D protein map of four different subunits of the centriole could be obtained. Panel d adapted with permission from Reference 120. (e) The orientation of different components of the synaptonemal complex was determined by epitope tagging on both the N and C termini and 3D dual-color SMLM. Panel e adapted with permission from Reference 65.

CONCLUSION

New developments in SMLM have pushed its resolution toward the single-nanometer scale. Thus, it can now optimally complement structural biology techniques such as cryo-EM by extracting relative positions of labeled epitopes in intact cells, even for structures that are too complex or dynamic to be resolved in cryo-EM with atomic resolution. Correlative SMLM and EM (29)

directly combine the power of SRM in imaging whole cells and tissues at the molecular scale with molecular specificity and the ability to determine atomic structure. In the future, use of the fluorescence signal to identify and segment structures of interest, to classify molecular machines according to their functional state, and as an additional constraint in model building will have countless applications across the life sciences.

To fully exploit the potential of SMLM for structural cell biology, the resolution, live-cell compatibility, and multicolor imaging aspects of this technique require further improvement. In terms of resolution, DNA-PAINT and MINFLUX achieve down to 2 nm localization precisions from a single emission event, leaving microscope instabilities and linkage errors as the main limitations to resolution. System stability can become the major limitation to ultraprecision SMLM and MINFLUX imaging, and active stabilization and ultraprecise drift correction are often indispensable. Linkage errors can potentially be overcome by using unnatural amino acids for labeling.

MINFLUX has the potential to achieve the highest resolution of all SRM imaging techniques, even with photoswitchable fluorescent proteins, and for tiny FoVs, it can in principle be very fast. For larger fields, however, the throughput is currently low, and current MINFLUX implementations tend to detect fewer fluorophores compared to camera-based (wide-field) SMLM techniques. Improving the imaging speed and localization robustness would be highly desirable for future developments of MINFLUX imaging, especially with regards to dynamic live-cell MINFLUX.

In spite of all the excitement around MINFLUX, camera-based SMLM techniques, with their high throughput and mature data acquisition and analysis pipelines, will stay relevant for collecting large amounts of data, e.g., for particle averaging or dynamic reconstructions, detecting rare events, or performing statistically powerful analyses.

Many of the current limitations for high-resolution live-cell and multicolor imaging are based on available fluorophores. Engineering bright, multicolor, reactivatable and live cell-compatible fluorophores and labeling techniques will be the major driving forces pushing SMLM toward dynamic structural biology.

With these developments, SRM will likely become a key complementary technology for structural cell biology to investigate the structure and dynamics of molecular machines in the living cell.

SUMMARY POINTS

1. Super-resolution microscopy can reach close to molecular-scale resolution, thereby complementing standard techniques used in structural biology.
2. New single-molecule localization microscopy (SMLM) approaches can achieve a resolution below 10 nm in 3D and multicolor imaging.
3. Resolution in SMLM is determined by the optical setup, the choice of fluorophores, the labeling schemes, the imaging conditions, and the stability of the microscope.
4. Examples that used SMLM for structural analysis include studies of the axonal actin-spectrin cytoskeleton, the nuclear pore complex, the endocytic machinery, the centriole, and the synaptonemal complex.
5. Minimal photon flux (MINFLUX) is a new live cell-compatible super-resolution technique combining switching of fluorophores and donut-shaped excitation for imaging with the highest resolution currently possible and tracking with high speed and precision.

6. Quantitative data analysis like particle averaging or model fitting is crucial to obtain structural information from SMLM data sets.

FUTURE ISSUES

1. Engineering bright, reactivatable, and live cell-compatible synthetic fluorophores and fluorescent proteins will be a major driving force to push SMLM and MINFLUX toward dynamic structural biology.
2. Future developments of high-speed MINFLUX will enable taking time-lapse movies of molecular machines. Such developments include fluorophore engineering; improved optics, electronics, and software; and optimization of imaging and sample preparation conditions.
3. To achieve molecular-scale precision (1–5 nm), both MINFLUX and camera-based SMLM techniques require subnanometer system stability, where vibration and drift need to be fully evaluated and compensated either with active stabilization systems or with ultraprecise drift correction.
4. Correlative cryo-SMLM and cryo-EM could revolutionize structural biology by combining molecular specificity of the fluorescence label with true structural resolution, but this will require the development of stable cryo-microscopes with efficient heat transfer to prevent devitrification from optical illumination, fluorophores that switch at cryogenic temperatures, and data registration with nanometer accuracy.
5. As the resolution reaches molecular scales, labeling of the target structure with minimal linkage error with, e.g., unnatural amino acids, needs to become routine, and new labeling schemes need to be developed.

DISCLOSURE STATEMENT

The authors are not aware of any affiliations, memberships, funding, or financial holdings that might be perceived as affecting the objectivity of this review.

LITERATURE CITED

1. Altman RB, Terry DS, Zhou Z, Zheng Q, Geggier P, et al. 2012. Cyanine fluorophore derivatives with enhanced photostability. *Nat. Methods* 9:68–71
2. Annibale P, Vanni S, Scarselli M, Rothlisberger U, Radenovic A. 2011. Quantitative photo activated localization microscopy: unraveling the effects of photoblinking. *PLOS ONE* 6(7):e22678
3. Aquino D, Schönle A, Geisler C, von Middendorff C, Wurm CA, et al. 2011. Two-color nanoscopy of three-dimensional volumes by 4Pi detection of stochastically switched fluorophores. *Nat. Methods* 8(4):353–59
4. Babcock HP, Zhuang X. 2017. Analyzing single molecule localization microscopy data using cubic splines. *Sci. Rep.* 7:552
5. Balinovic A, Albrecht D, Endesfelder U. 2019. Spectrally red-shifted fluorescent fiducial markers for optimal drift correction in localization microscopy. *J. Phys. D* 52:204002
6. Balzarotti F, Eilers Y, Gwosch KC, Gynnå AH, Westphal V, et al. 2017. Nanometer resolution imaging and tracking of fluorescent molecules with minimal photon fluxes. *Science* 355(6325):606–12

7. Barasoain I, Díaz JF, Andreu JM. 2010. Fluorescent taxoid probes for microtubule research. *Methods Cell Biol.* 95:353–72
8. Barentine AES, Lin Y, Liu M, Kidd P, Balduf L, et al. 2019. 3D multicolor nanoscopy at 10,000 cells a day. bioRxiv 606954. <https://doi.org/10.1101/606954>
9. Bates M, Huang B, Dempsey GT, Zhuang X. 2007. Multicolor super-resolution imaging with photo-switchable fluorescent probes. *Science* 317(5845):1749–53
10. Beghin A, Kechkar A, Butler C, Levet F, Cabillic M, et al. 2017. Localization-based super-resolution imaging meets high-content screening. *Nat. Methods* 14(12):1184–90
11. Beliu G, Kurz AJ, Kuhlemann AC, Behringer-Pliess L, Meub M, et al. 2019. Bioorthogonal labeling with tetrazine-dyes for super-resolution microscopy. *Commun. Biol.* 2:261
12. Benesch RE, Benesch R. 1953. Enzymatic removal of oxygen for polarography and related methods. *Science* 118(3068):447–48
13. Betzig E, Patterson GH, Sougrat R, Lindwasser OW, Olenych S, et al. 2006. Imaging intracellular fluorescent proteins at nanometer resolution. *Science* 313(5793):1642–45
14. Bock H, Geisler C, Wurm CA, von Middendorff C, Jakobs S, et al. 2007. Two-color far-field fluorescence nanoscopy based on photoswitchable emitters. *Appl. Phys. B* 88(2):161–65
15. Bon P, Bourg N, Lécart S, Monneret S, Fort E, et al. 2015. Three-dimensional nanometre localization of nanoparticles to enhance super-resolution microscopy. *Nat. Commun.* 6:7764
16. Bon P, Linares-Loyez J, Feyeux M, Alessandri K, Lounis B, et al. 2018. Self-interference 3D super-resolution microscopy for deep tissue investigations. *Nat. Methods* 15(6):449–54
17. Bornens M. 2012. The centrosome in cells and organisms. *Science* 335(6067):422–26
18. Bossi M, Fölling J, Belov VN, Boyarskiy VP, Medda R, et al. 2008. Multicolor far-field fluorescence nanoscopy through isolated detection of distinct molecular species. *Nano Lett.* 8(8):2463–68
19. Bourg N, Mayet C, Dupuis G, Barroca T, Bon P, et al. 2015. Direct optical nanoscopy with axially localized detection. *Nat. Photon.* 9(9):587–93
20. Bowler M, Kong D, Sun S, Nanjundappa R, Evans L, et al. 2019. High-resolution characterization of centriole distal appendage morphology and dynamics by correlative STORM and electron microscopy. *Nat. Commun.* 10:993
21. Briggs JA. 2013. Structural biology in situ—the potential of subtomogram averaging. *Curr. Opin. Struct. Biol.* 23(2):261–67
22. Broeken J, Johnson H, Lidke DS, Liu S, Nieuwenhuizen RPJ, et al. 2015. Resolution improvement by 3D particle averaging in localization microscopy. *Methods Appl. Fluoresc.* 3(1):014003
23. Carrington G, Tomlinson D, Peckham M. 2019. Exploiting nanobodies and affimers for superresolution imaging in light microscopy. *Mol. Biol. Cell* 30(22):2737–40
24. Cheng Y, Grigorieff N, Penczek PA, Walz T. 2015. A primer to single-particle cryo-electron microscopy. *Cell* 161(3):438–49
25. Cnossen J, Cui TJ, Joo C, Smith C. 2021. Drift correction in localization microscopy using entropy minimization. *Opt. Express* 29(18):27961–74
26. Cnossen J, Hinsdale T, Thorsen RØ, Siemons M, Schueder F, et al. 2020. Localization microscopy at doubled precision with patterned illumination. *Nat. Methods* 17:59–63
27. Coelho S, Baek J, Graus MS, Halstead JM, Nicovich PR, et al. 2020. Ultraprecise single-molecule localization microscopy enables in situ distance measurements in intact cells. *Sci. Adv.* 6(16):eaay8271
28. Coelho S, Baek J, Walsh J, Gooding JJ, Gaus K. 2021. 3D active stabilization for single-molecule imaging. *Nat. Protoc.* 16:497–515
29. Dahlberg PD, Moerner WE. 2021. Cryogenic super-resolution fluorescence and electron microscopy correlated at the nanoscale. *Annu. Rev. Phys. Chem.* 72:253–78
30. Dasgupta A, Deschamps J, Matti U, Hübner U, Becker J, et al. 2021. Direct supercritical angle localization microscopy for nanometer 3D superresolution. *Nat. Commun.* 12:1180
31. Dempsey GT, Vaughan JC, Chen KH, Bates M, Zhuang X. 2011. Evaluation of fluorophores for optimal performance in localization-based super-resolution imaging. *Nat. Methods* 8(12):1027–36
32. Deschamps J, Mund M, Ries J. 2014. 3D superresolution microscopy by supercritical angle detection. *Opt. Express* 22(23):29081–91

33. Deschamps J, Rowald A, Ries J. 2016. Efficient homogeneous illumination and optical sectioning for quantitative single-molecule localization microscopy. *Opt. Express* 24(24):28080–90
34. Diekmann R, Kahnwald M, Schoenit A, Deschamps J, Matti U, Ries J. 2020. Optimizing imaging speed and excitation intensity for single-molecule localization microscopy. *Nat. Methods* 17(9):909–12
35. Douglass KM, Sieben C, Archetti A, Lambert A, Manley S. 2016. Super-resolution imaging of multiple cells by optimized flat-field epi-illumination. *Nat. Photon.* 10(11):705–8
36. Durisic N, Laparra-Cuervo L, Sandoval-Álvarez Á, Borbely JS, Lakadamyali M. 2014. Single-molecule evaluation of fluorescent protein photoactivation efficiency using an in vivo nanotemplate. *Nat. Methods* 11(2):156–62
37. Eilers Y, Ta H, Gwosch KC, Balzarotti F, Hell SW. 2018. MINFLUX monitors rapid molecular jumps with superior spatiotemporal resolution. *PNAS* 115(24):6117–22
38. Fernández-Suárez M, Ting AY. 2008. Fluorescent probes for super-resolution imaging in living cells. *Nat. Rev. Mol. Cell Biol.* 9(12):929–43
39. Finan K, Raulf A, Heilemann M. 2015. A set of homo-oligomeric standards allows accurate protein counting. *Angew. Chem. Int. Ed.* 54(41):12049–52
40. Früh SM, Matti U, Spycher PR, Rubini M, Lickert S, et al. 2021. Site-specifically-labeled antibodies for super-resolution microscopy reveal in situ linkage errors. *ACS Nano* 15(7):12161–70
41. Früh SM, Schoen I, Ries J, Vogel V. 2015. Molecular architecture of native fibronectin fibrils. *Nat. Commun.* 6:7275
42. Gautier A, Juillerat A, Heinis C, Corrêa IR, Kindermann M, et al. 2008. An engineered protein tag for multiprotein labeling in living cells. *Chem. Biol.* 15(2):128–36
43. Goodsell DS, Autin L, Olson AJ. 2019. Illustrate: software for biomolecular illustration. *Structure* 27(11):1716–20.e1
44. Götzke H, Kilisch M, Martínez-Carranza M, Sograte-Idrissi S, Rajavel A, et al. 2019. The ALFA-tag is a highly versatile tool for nanobody-based bioscience applications. *Nat. Commun.* 10:4403
45. Grimm JB, English BP, Chen J, Slaughter JP, Zhang Z, et al. 2015. A general method to improve fluorophores for live-cell and single-molecule microscopy. *Nat. Methods* 12(3):244–50
46. Grimm JB, English BP, Choi H, Muthusamy AK, Mehl BP, et al. 2016. Bright photoactivatable fluorophores for single-molecule imaging. *Nat. Methods* 13(12):985–88
47. Gu L, Li Y, Zhang S, Xue Y, Li W, et al. 2019. Molecular resolution imaging by repetitive optical selective exposure. *Nat. Methods* 16(11):1114–18
48. Gu L, Li Y, Zhang S, Zhou M, Xue Y, et al. 2021. Molecular-scale axial localization by repetitive optical selective exposure. *Nat. Methods* 18(4):369–73
49. Gwosch KC, Pape JK, Balzarotti F, Hoess P, Ellenberg J, et al. 2020. MINFLUX nanoscopy delivers 3D multicolor nanometer resolution in cells. *Nat. Methods* 17(2):217–24
50. Hajj B, Wisniewski J, Beheiry ME, Chen J, Revyakin A, et al. 2014. Whole-cell, multicolor superresolution imaging using volumetric multifocus microscopy. *PNAS* 111(49):17480–85
51. Hauser M, Wojcik M, Kim D, Mahmoudi M, Li W, Xu K. 2017. Correlative super-resolution microscopy: new dimensions and new opportunities. *Chem. Rev.* 117(11):7428–56
52. Heilemann M, van de Linde S, Schüttelz M, Kasper R, Seefeldt B, et al. 2008. Subdiffraction-resolution fluorescence imaging with conventional fluorescent probes. *Angew. Chem. Int. Ed.* 47(33):6172–76
53. Hess ST, Girirajan TPK, Mason MD. 2006. Ultra-high resolution imaging by fluorescence photoactivation localization microscopy. *Biophys. J.* 91(11):4258–72
54. Heydarian H, Joosten M, Przybylski A, Schueder F, Jungmann R, et al. 2021. 3D particle averaging and detection of macromolecular symmetry in localization microscopy. *Nat. Commun.* 12:2847
55. Heydarian H, Schueder F, Strauss MT, van Werkhoven B, Fazel M, et al. 2018. Template-free 2D particle fusion in localization microscopy. *Nat. Methods* 15(10):781–84
56. Hoess P, Mund M, Reitberger M, Ries J. 2018. Dual-color and 3D super-resolution microscopy of multi-protein assemblies. *Methods Mol. Biol.* 1764:237–51

40. Quantification of linkage error in SMLM.

48. Demonstrated that ROSE-z achieves comparable performance with 4Pi-SMLM using axially modulated illumination.

49. Extension of MINFLUX to large FoVs and to 3D, dual-color, and live cells.

52. Established dSTORM as an experimentally simpler version of STORM.

54. Template-free 3D particle averaging for SMLM.

63. 3D whole-cell imaging at 10 nm resolution using 4Pi-SMLM.

71. Established DNA-PAINT and the corresponding multiplexing.

57. Hoffman DP, Shtengel G, Xu CS, Campbell KR, Freeman M, et al. 2020. Correlative three-dimensional super-resolution and block-face electron microscopy of whole vitreously frozen cells. *Science* 367(6475):eaaz5357
58. Holden SJ, Pengo T, Meibom KL, Fernandez CF, Collier J, Manley S. 2014. High throughput 3D super-resolution microscopy reveals *Caulobacter crescentus* in vivo Z-ring organization. *PNAS* 111(12):4566–71
59. Holden SJ, Uphoff S, Kapanidis AN. 2011. DAOSTORM: an algorithm for high-density super-resolution microscopy. *Nat. Methods* 8(4):279–80
60. Huang B, Wang W, Bates M, Zhuang X. 2008. Three-dimensional super-resolution imaging by stochastic optical reconstruction microscopy. *Science* 319(5864):810–13
61. Huang F, Hartwich TMP, Rivera-Molina FE, Lin Y, Duim WC, et al. 2013. Video-rate nanoscopy using sCMOS camera-specific single-molecule localization algorithms. *Nat. Methods* 10(7):653–58
62. Huang F, Schwartz SL, Byars JM, Lidke KA. 2011. Simultaneous multiple-emitter fitting for single molecule super-resolution imaging. *Biomed. Opt. Express* 2(5):1377–93
63. **Huang F, Sirinakis G, Allgeyer ES, Schroeder LK, Duim WC, et al. 2016. Ultra-high resolution 3D imaging of whole cells. *Cell* 166(4):1028–40**
64. Huhle A, Klaue D, Brutzer H, Daldrop P, Joo S, et al. 2015. Camera-based three-dimensional real-time particle tracking at kHz rates and Ångström accuracy. *Nat. Commun.* 6:5885
65. Hurlock ME, Čavka I, Kursel LE, Haversat J, Wooten M, et al. 2020. Identification of novel synaptone-mal complex components in *C. elegans*. *J. Cell Biol.* 219(5):e20190043
66. Isselstein M, Zhang L, Glembockyte V, Brix O, Cosa G, et al. 2020. Self-healing dyes—keeping the promise? *J. Phys. Chem. Lett.* 11(11):4462–80
67. Jimenez Sabinina V, Hossain MJ, Hériché J-K, Hoess P, Nijmeijer B, et al. 2021. Three-dimensional superresolution fluorescence microscopy maps the variable molecular architecture of the nuclear pore complex. *Mol. Biol. Cell* 32(17):1523–33
68. Jouchet P, Gabriel C, Bourg N, Bardou M, Poüs C, et al. 2021. Nanometric axial localization of single fluorescent molecules with modulated excitation. *Nat. Photon.* 15:297–304
69. Juette MF, Gould TJ, Lessard MD, Mlodzianoski MJ, Nagpure BS, et al. 2008. Three-dimensional sub-100 nm resolution fluorescence microscopy of thick samples. *Nat. Methods* 5(6):527–29
70. Jungmann R, Avendaño MS, Dai M, Woehrstein JB, Agasti SS, et al. 2016. Quantitative super-resolution imaging with qPAINT. *Nat. Methods* 13(5):439–42
71. **Jungmann R, Avendaño MS, Woehrstein JB, Dai M, Shih WM, Yin P. 2014. Multiplexed 3D cellular super-resolution imaging with DNA-PAINT and Exchange-PAINT. *Nat. Methods* 11(3):313–18**
72. Kanchanawong P, Shtengel G, Pasapera AM, Ramko EB, Davidson MW, et al. 2010. Nanoscale architecture of integrin-based cell adhesions. *Nature* 468(7323):580–84
73. Keppler A, Gendreizig S, Gronemeyer T, Pick H, Vogel H, Johnsson K. 2003. A general method for the covalent labeling of fusion proteins with small molecules in vivo. *Nat. Biotechnol.* 21(1):86–89
74. Kim D, Deerinck TJ, Sigal YM, Babcock HP, Ellisman MH, Zhuang X. 2015. Correlative stochastic optical reconstruction microscopy and electron microscopy. *PLOS ONE* 10(4):e0124581
75. Klehs K, Spahn C, Endesfelder U, Lee SF, Fürstenberg A, Heilemann M. 2014. Increasing the brightness of cyanine fluorophores for single-molecule and superresolution imaging. *Chem. Phys. Chem.* 15(4):637–41
76. Köhler S, Wojcik M, Xu K, Dernburg AF. 2017. Superresolution microscopy reveals the three-dimensional organization of meiotic chromosome axes in intact *Caenorhabditis elegans* tissue. *PNAS* 114(24):E4734–43
77. Kopek BG, Paez-Segala MG, Shtengel G, Sochacki KA, Sun MG, et al. 2017. Diverse protocols for correlative super-resolution fluorescence imaging and electron microscopy of chemically fixed samples. *Nat. Protoc.* 12(5):916–46
78. Laplante C, Huang F, Tebbs IR, Bewersdorf J, Pollard TD. 2016. Molecular organization of cytokinesis nodes and contractile rings by super-resolution fluorescence microscopy of live fission yeast. *PNAS* 113(40):E5876–85
79. Lardon N, Wang L, Tschanz A, Hoess P, Tran M, et al. 2021. Systematic tuning of rhodamine spirocyclization for super-resolution microscopy. *J. Am. Chem. Soc.* 143(36):14592–600

80. Lee SF, Vérolet Q, Fürstenberg A. 2013. Improved super-resolution microscopy with oxazine fluorophores in heavy water. *Angew. Chem. Int. Ed.* 52(34):8948–51
81. Lee S-H, Shin JY, Lee A, Bustamante C. 2012. Counting single photoactivatable fluorescent molecules by photoactivated localization microscopy (PALM). *PNAS* 109(43):17436–41
82. Lelek M, Gyparaki MT, Beliu G, Schueder F, Griffié J, et al. 2021. Single-molecule localization microscopy. *Nat. Rev. Methods Primers* 1:39
83. Li Y, Mund M, Hoess P, Deschamps J, Matti U, et al. 2018. Real-time 3D single-molecule localization using experimental point spread functions. *Nat. Methods* 15(5):367–69
84. Lin Y, Long JJ, Huang F, Duim WC, Kirschbaum S, et al. 2015. Quantifying and optimizing single-molecule switching nanoscopy at high speeds. *PLOS ONE* 10(5):e0128135
85. Liu S, Huang F. 2020. Enhanced 4Pi single-molecule localization microscopy with coherent pupil based localization. *Commun. Biol.* 3:220
86. Los GV, Encell LP, McDougall MG, Hartzell DD, Karassina N, et al. 2008. HaloTag: a novel protein labeling technology for cell imaging and protein analysis. *ACS Chem. Biol.* 3(6):373–82
87. Löschberger A, Franke C, Krohne G, van de Linde S, Sauer M. 2014. Correlative super-resolution fluorescence and electron microscopy of the nuclear pore complex with molecular resolution. *J. Cell Sci.* 127(20):4351–55
88. Löschberger A, van de Linde S, Dabauvalle M-C, Rieger B, Heilemann M, et al. 2012. Super-resolution imaging visualizes the eightfold symmetry of gp210 proteins around the nuclear pore complex and resolves the central channel with nanometer resolution. *J. Cell Sci.* 125(3):570–75
89. McEvoy AL, Hoi H, Bates M, Platonova E, Cranfill PJ, et al. 2012. mMaple: a photoconvertible fluorescent protein for use in multiple imaging modalities. *PLOS ONE* 7(12):e51314
90. McGorty R, Kamiyama D, Huang B. 2013. Active microscope stabilization in three dimensions using image correlation. *Opt. Nanosc.* 2(1):10
91. Mlodzianoski MJ, Schreiner JM, Callahan SP, Smolková K, Dlasková A, et al. 2011. Sample drift correction in 3D fluorescence photoactivation localization microscopy. *Opt. Express* 19(16):15009–19
92. Möckl L, Moerner WE. 2020. Super-resolution microscopy with single molecules in biology and beyond: essentials, current trends, and future challenges. *J. Am. Chem. Soc.* 142(42):17828–44
93. M'Saad O, Bewersdorf J. 2020. Light microscopy of proteins in their ultrastructural context. *Nat. Commun.* 11:3850
- 94. Mund M, van der Beek JA, Deschamps J, Dmitrieff S, Hoess P, et al. 2018. Systematic nanoscale analysis of endocytosis links efficient vesicle formation to patterned actin nucleation. *Cell* 174(4):884–96.e17**
95. Nehme E, Freedman D, Gordon R, Ferdman B, Weiss LE, et al. 2020. DeepSTORM3D: dense 3D localization microscopy and PSF design by deep learning. *Nat. Methods* 17:734–40
96. Nieuwenhuizen RPJ, Bates M, Szymborska A, Lidke KA, Rieger B, Stallinga S. 2015. Quantitative localization microscopy: effects of photophysics and labeling stoichiometry. *PLOS ONE* 10(5):e0127989
97. Olivier N, Keller D, Gönczy P, Manley S. 2013. Resolution doubling in 3D-STORM imaging through improved buffers. *PLOS ONE* 8(7):e69004
98. Ong WQ, Citron YR, Schnitzbauer J, Kamiyama D, Huang B. 2015. Heavy water: a simple solution to increasing the brightness of fluorescent proteins in super-resolution imaging. *Chem. Commun.* 51(70):13451–53
99. Opazo F, Levy M, Byrom M, Schäfer C, Geisler C, et al. 2012. Aptamers as potential tools for super-resolution microscopy. *Nat. Methods* 9(10):938–39
100. Pape JK, Stephan T, Balzarotti F, Büchner R, Lange F, et al. 2020. Multicolor 3D MINFLUX nanoscopy of mitochondrial MICOS proteins. *PNAS* 117(34):20607–14
101. Pavani SRP, Thompson MA, Biteen JS, Lord SJ, Liu N, et al. 2009. Three-dimensional, single-molecule fluorescence imaging beyond the diffraction limit by using a double-helix point spread function. *PNAS* 106(9):2995–99
102. Pertsinidis A, Zhang Y, Chu S. 2010. Subnanometre single-molecule localization, registration and distance measurements. *Nature* 466(7306):647–51

94. Protein organization and assembly at endocytic sites in yeast cells using particle averaging and dynamic reconstruction.

103. Puchner EM, Walter JM, Kasper R, Huang B, Lim WA. 2013. Counting molecules in single organelles with superresolution microscopy allows tracking of the endosome maturation trajectory. *PNAS* 110(40):16015–20
104. Punjani A, Rubinstein JL, Fleet DJ, Brubaker MA. 2017. cryoSPARC: algorithms for rapid unsupervised cryo-EM structure determination. *Nat. Methods* 14(3):290–96
105. Reymond L, Huser T, Ruprecht V, Wieser S. 2020. Modulation-enhanced localization microscopy. *J. Phys. Photon.* 2(4):041001
106. Reymond L, Ziegler J, Knapp C, Wang F-C, Huser TR, et al. 2019. SIMPLE: structured illumination based point localization estimator with enhanced precision. *Opt. Express* 27(17):24578–90
107. Ries J, Kaplan C, Platonova E, Eghlidi H, Ewers H. 2012. A simple, versatile method for GFP-based super-resolution microscopy via nanobodies. *Nat. Methods* 9(6):582–84
108. Rollins GC, Shin JY, Bustamante C, Pressé S. 2015. Stochastic approach to the molecular counting problem in superresolution microscopy. *PNAS* 112(2):E110–18
109. Ruckstuhl T, Verdes D. 2004. Supercritical angle fluorescence (SAF) microscopy. *Opt. Express* 12(18):4246–54
110. Rust MJ, Bates M, Zhuang X. 2006. Sub-diffraction-limit imaging by stochastic optical reconstruction microscopy (STORM). *Nat. Methods* 3(10):793–96
111. Schlichthaerle T, Eklund AS, Schueder F, Strauss MT, Tiede C, et al. 2018. Site-specific labeling of affimers for DNA-PAINT microscopy. *Angew. Chem. Int. Ed.* 57(34):11060–63
112. Schmidt R, Weihs T, Wurm CA, Jansen I, Rehman J, et al. 2021. MINFLUX nanometer-scale 3D imaging and microsecond-range tracking on a common fluorescence microscope. *Nat. Commun.* 12:1478
113. Schnitzbauer J, Strauss MT, Schlichthaerle T, Schueder F, Jungmann R. 2017. Super-resolution microscopy with DNA-PAINT. *Nat. Protoc.* 12(6):1198–228
114. Schnitzbauer J, Wang Y, Zhao S, Bakalar M, Nuwal T, et al. 2018. Correlation analysis framework for localization-based superresolution microscopy. *PNAS* 115(3):3219–24
115. Sharonov A, Hochstrasser RM. 2006. Wide-field subdiffraction imaging by accumulated binding of diffusing probes. *PNAS* 103(50):18911–16
116. Shechtman Y, Weiss LE, Backer AS, Sahl SJ, Moerner WE. 2015. Precise three-dimensional scan-free multiple-particle tracking over large axial ranges with tetrapod point spread functions. *Nano Lett.* 15(6):4194–99
117. Shi X, Garcia G, Van De Weghe JC, McGorty R, Pazour GJ, et al. 2017. Super-resolution microscopy reveals that disruption of ciliary transition-zone architecture causes Joubert syndrome. *Nat. Cell Biol.* 19(10):1178–88
118. Shroff H, Galbraith CG, Galbraith JA, White H, Gillette JM, et al. 2007. Dual-color superresolution imaging of genetically expressed probes within individual adhesion complexes. *PNAS* 104(51):20308–13
119. Shtengel G, Galbraith JA, Galbraith CG, Lippincott-Schwartz J, Gillette JM, et al. 2009. Interferometric fluorescent super-resolution microscopy resolves 3D cellular ultrastructure. *PNAS* 106(9):3125–30
120. Sieben C, Banterle N, Douglass KM, Gönczy P, Manley S. 2018. Multicolor single-particle reconstruction of protein complexes. *Nat. Methods* 15(10):777–80
121. Sillibourne JE, Specht CG, Izeddin I, Hurbain I, Tran P, et al. 2011. Assessing the localization of centrosomal proteins by PALM/STORM nanoscopy. *Cytoskeleton* 68(11):619–27
122. Sochacki KA, Dickey AM, Strub M-P, Taraska JW. 2017. Endocytic proteins are partitioned at the edge of the clathrin lattice in mammalian cells. *Nat. Cell Biol.* 19(4):352–61
123. Speiser A, Müller L-R, Hoess P, Matti U, Obara CJ, et al. 2021. Deep learning enables fast and dense single-molecule localization with high accuracy. *Nat. Methods* 18:1082–90
124. Stehr F, Stein J, Schueder F, Schwille P, Jungmann R. 2019. Flat-top TIRF illumination boosts DNA-PAINT imaging and quantification. *Nat. Commun.* 10:1268
125. Szymborska A, de Marco A, Daigle N, Cordes VC, Briggs JAG, Ellenberg J. 2013. Nuclear pore scaffold structure analyzed by super-resolution microscopy and particle averaging. *Science* 341(6146):655–58
126. Takakura H, Zhang Y, Erdmann RS, Thompson AD, Lin Y, et al. 2017. Long time-lapse nanoscopy with spontaneously blinking membrane probes. *Nat. Biotechnol.* 35(8):773–80
127. Tam J, Cordier GA, Borbely JS, Álvarez AS, Lakadamyali M. 2014. Cross-talk-free multi-color STORM imaging using a single fluorophore. *PLOS ONE* 9(7):e101772

128. Testa I, Wurm CA, Medda R, Rothermel E, von Middendorff C, et al. 2010. Multicolor fluorescence nanoscopy in fixed and living cells by exciting conventional fluorophores with a single wavelength. *Biophys. J.* 99(8):2686–94
129. Thevathasan JV, Kahnwald M, Cieśliński K, Hoess P, Peneti SK, et al. 2019. Nuclear pores as versatile reference standards for quantitative superresolution microscopy. *Nat. Methods* 16(10):1045–53
130. Traenkle B, Rothbauer U. 2017. Under the microscope: single-domain antibodies for live-cell imaging and super-resolution microscopy. *Front. Immunol.* 8:1030
131. Turkowyd B, Balinovic A, Virant D, Carnero HGG, Caldana F, et al. 2017. A general mechanism of photoconversion of green-to-red fluorescent proteins based on blue and infrared light reduces phototoxicity in live-cell single-molecule imaging. *Angew. Chem. Int. Ed.* 56(38):11634–39
132. Uno S, Kamiya M, Yoshihara T, Sugawara K, Okabe K, et al. 2014. A spontaneously blinking fluorophore based on intramolecular spirocyclization for live-cell super-resolution imaging. *Nat. Chem.* 6(8):681–89
133. Uttamapinant C, Howe JD, Lang K, Beránek V, Davis L, et al. 2015. Genetic code expansion enables live-cell and super-resolution imaging of site-specifically labeled cellular proteins. *J. Am. Chem. Soc.* 137(14):4602–5
134. Valley CC, Liu S, Lidke DS, Lidke KA. 2015. Sequential superresolution imaging of multiple targets using a single fluorophore. *PLoS ONE* 10(4):e0123941
135. Vicidomini G, Bianchini P, Diaspro A. 2018. STED super-resolved microscopy. *Nat. Methods* 15(3):173–82
136. Virant D, Traenkle B, Maier J, Kaiser PD, Bodenhofer M, et al. 2018. A peptide tag-specific nanobody enables high-quality labeling for dSTORM imaging. *Nat. Commun.* 9:930
137. Virant D, Turkowyd B, Balinovic A, Endesfelder U. 2017. Combining primed photoconversion and UV-photoactivation for aberration-free, live-cell compliant multi-color single-molecule localization microscopy imaging. *Int. J. Mol. Sci.* 18(7):1524
138. Vogelsang J, Kasper R, Steinhauer C, Person B, Heilemann M, et al. 2008. A reducing and oxidizing system minimizes photobleaching and blinking of fluorescent dyes. *Angew. Chem. Int. Ed.* 47(29):5465–69
139. von Appen A, Kosinski J, Sparks L, Ori A, DiGuilio AL, et al. 2015. In situ structural analysis of the human nuclear pore complex. *Nature* 526(7571):140–43
140. Wang J, Allgeyer ES, Sirinakis G, Zhang Y, Hu K, et al. 2021. Implementation of a 4Pi-SMS super-resolution microscope. *Nat. Protoc.* 16(2):677–727
141. Wang L, Frei MS, Salim A, Johnsson K. 2019. Small-molecule fluorescent probes for live-cell super-resolution microscopy. *J. Am. Chem. Soc.* 141(7):2770–81
142. Wang Y, Schnitzbauer J, Hu Z, Li X, Cheng Y, et al. 2014. Localization events-based sample drift correction for localization microscopy with redundant cross-correlation algorithm. *Opt. Express* 22(13):15982–91
143. Wassie AT, Zhao Y, Boyden ES. 2018. Expansion microscopy: principles and uses in biological research. *Nat. Methods* 16(1):33–41
144. Weisenburger S, Boening D, Schomburg B, Giller K, Becker S, et al. 2017. Cryogenic optical localization provides 3D protein structure data with Angstrom resolution. *Nat. Methods* 14(2):141–44
145. Wu Y-L, Hoess P, Tschanz A, Matti U, Mund M, Ries J. 2021. Maximum-likelihood model fitting for quantitative analysis of SMLM data. bioRxiv 2021.08.30.456756. <https://doi.org/10.1101/2021.08.30.456756>
146. Wu Y-L, Tschanz A, Krupnik L, Ries J. 2020. Quantitative data analysis in single-molecule localization microscopy. *Trends Cell Biol.* 30(11):837–51
147. Wulf E, Deboben A, Bautz FA, Faulstich H, Wieland T. 1979. Fluorescent phalloxin, a tool for the visualization of cellular actin. *PNAS* 76(9):4498–502
148. Xu K, Zhong G, Zhuang X. 2013. Actin, spectrin, and associated proteins form a periodic cytoskeletal structure in axons. *Science* 339(6118):452–56
149. Znacchi FC, Manzo C, Alvarez AS, Derr ND, Garcia-Parajo MF, Lakadamyali M. 2017. A DNA origami platform for quantifying protein copy number in super-resolution. *Nat. Methods* 14(8):789–92

129. Introduced NPC cell lines as a reference standard for resolution, counting, and labeling in SMLM.

148. Discovered the periodic organization of actin and spectrin in axons using dual-objective SMLM.

150. Zhang M, Chang H, Zhang Y, Yu J, Wu L, et al. 2012. Rational design of true monomeric and bright photoactivatable fluorescent proteins. *Nat. Methods* 9(7):727–29
151. Zhang Y, Schroeder LK, Lessard MD, Kidd P, Chung J, et al. 2020. Nanoscale subcellular architecture revealed by multicolor three-dimensional salvaged fluorescence imaging. *Nat. Methods* 17(2):225–31
152. Zhao T, Wang Y, Zhai Y, Qu X, Cheng A, et al. 2015. A user-friendly two-color super-resolution localization microscope. *Opt. Express* 23(2):1879–87
153. Zhu L, Zhang W, Elnatan D, Huang B. 2012. Faster STORM using compressed sensing. *Nat. Methods* 9(7):721–23
154. Zwettler FU, Reinhard S, Gambarotto D, Bell TDM, Hamel V, et al. 2020. Molecular resolution imaging by post-labeling expansion single-molecule localization microscopy (Ex-SMLM). *Nat. Commun.* 11:3388